Biochemistry

 Volume 23, Number 15 July 17, 1984

Articles

Localization of Lipoyl-Bearing Domains in the α-Ketoglutarate Dehydrogenase Multienzyme Complex†

Terence Wagenknecht* and Joachim Frank

ABSTRACT: The α-ketoglutarate dehydrogenase complex from *Escherichia coli* consists of a core component, dihydrolipoyl transsuccinylase (E2), to which are noncovalently bound 12 polypeptide chains each of α-ketoglutarate dehydrogenase and dihydrolipoyl dehydrogenase. E2 exists as a cube-shaped complex comprising 24 identical chains and may be resolved from the other two enzyme components. Limited digestion of E2 with trypsin quantitatively removes domains containing the lipoic acid cofactor while leaving the quaternary structure of the complex intact. Averages of native and trypsin-modified E2 were computed from images of single molecules obtained from electron micrographs of negatively stained specimens. The two averages were very similar and were in general agreement with a model determined previously by X-ray crystallography. However, detailed analysis of the difference image, obtained by subtracting the average of the trypsin-treated E2 from the native E2, showed extra stain-excluding regions along the edges of the native molecule which we interpret as representing the lipoyl-bearing domains. Micrographs of mixtures of native and modified E2 were also analyzed in order to rule out staining or electron-optical artifacts as accounting for the results. On the basis of these results along with other available structural information, we propose that one function of the lipoyl domains is to permit interactions between distantly separated lipoyl moieties in the E2 complex; this proposal also agrees with recent results of modeling studies of biochemical data [Hackert, M. L., Oliver, R. M., & Reed, L. J. (1983) *Proc. Natl. Acad. Sci. U.S.A. 80*, 2226–2230].

The α-ketoglutarate dehydrogenase multienzyme complex (KGDC)[1] from *Escherichia coli* comprises three enzymes which are all present in multiple copies (Pettit et al., 1973): 12 chains of α-ketoglutarate dehydrogenase (EC 1.2.4.2) (E1), 24 chains of dihydrolipoyl transsuccinylase (EC 2.3.1.61) (E2), and 12 chains of dihydrolioyl dehydrogenase (EC 1.6.4.3) (E3). The three enzymes, acting in sequence, catalyze the following overall reaction:

$$HO_2CCH_2CH_2COCO_2H + CoA\text{-}SH + NAD^+ \rightarrow HO_2CCH_2CH_2CO\text{-}S\text{-}CoA + CO_2 + NADH + H^+$$

E2 exists as a large complex (M_r 1 000 000) and serves as a structural core to which the other two enzyme components are bound (Reed & Oliver, 1968; Oliver & Reed, 1982). Overall the E2 molecule resembles a cube with truncated corners and has octahedral 432 symmetry. Most of the mass is located at the 24 vertices and along the edges; the interior and the faces of the molecule appear to be devoid of mass in the low-resolution structure determined by X-ray crystallography (DeRosier & Oliver, 1971; DeRosier et al., 1971; Hainfeld, 1974).

Each of the 24 identical polypeptide chains comprising the E2 complex bears a single lipoic acid moiety, which is believed to coordinate the action of the three component enzymes, being sufficiently mobile to transfer the various lipoyl-associated intermediates among the active centers of the KGDC (Collins & Reed, 1977; Angelides & Hammes, 1973). Originally it was hypothesized that the lipoyl lysine moieties themselves functioned as 1.4-nm-long "swinging arms" for this purpose (Koike et al., 1963), but more recent results indicate that the lipoyl lysines are attached to unusually mobile segments of polypeptide, so the arms may be considerably longer than was first believed (Stepp et al., 1981; Perham & Roberts, 1981). The lipoyl moieties form an interacting network capable of transferring both of the lipoyl-associated reaction intermediates, succinyl groups and electrons (Collins & Reed, 1977). Essentially identical observations apply to the lipoyl moieties of E2 of the pyruvate dehydrogenase complex from *Escher-*

† From the Center for Laboratories and Research, New York State Department of Health, Albany, New York 12201. *Received November 15, 1983.* This work was supported by Grant GM 29169 from the National Institutes of Health. A preliminary account of this work was presented (Wagenknecht & Frank, 1983).

[1] Abbreviations: E1, α-ketoglutarate dehydrogenase; E2, dihydrolipoyl transsuccinylase; E3, dihydrolipoyl dehydrogenase; KGDC, α-ketoglutarate dehydrogenase complex; t-E2, trypsin-modified E2; EDTA, ethylenediaminetetraacetic acid; $NaDodSO_4$, sodium dodecyl sulfate.

0006-2960/84/0423-3383$01.50/0

ichia coli (Collins & Reed, 1977; Stepp et al., 1981; Bates et al., 1977; Danson et al., 1978; Bleile et al., 1979; Perham et al., 1981) and may well be true of all α-ketoacid dehydrogenase complexes.

Treatment of the E2 complex with trypsin removes quantitatively a polypeptide associated with the lipoic acid cofactor (Stepp et al., 1981; Perham & Roberts, 1981; Bleile et al., 1979; Waskiewicz & Hammes, 1982). From E2 of the KGDC of *E. coli*, a polypeptide of ca. 11 kDa is released without disrupting the architecture of the enzyme complex. Alternatively, as we demonstrate here, the E2 complex may be resolved from the KGDC and then treated with protease, yielding a modified E2 complex (t-E2) identical with that found in the protease-treated KGDC. In this work, we have applied single-particle averaging methods (Frank et al., 1978; Frank, 1982) to electron micrographs of the isolated E2 complex and the protease-modified E2. Comparison of the averages for the two structures allowed us to map on the E2 molecule the site of the lipoyl-bearing domains. These domains are located, at least in part, approximately midway along the edges of the cube-shaped E2 complex.

Materials and Methods

Preparation of E2 and t-E2. KGDC was isolated from *Escherichia coli*, Crookes strain, and resolved into its three component enzymes by established procedures (Pettit et al., 1973; Reed & Mukherjee, 1969). Trypsin-modified E2 was prepared from the purified E2 by a procedure essentially identical with that reported for removing the lipoyl-bearing peptide from the KGDC (Stepp et al., 1981). To 150 μL of E2 at 5–10 mg/mL in 0.05 M potassium phosphate, pH 7.0, was added 150 μL of a freshly prepared solution consisting of 10 μg of trypsin/mL, 0.05 M phosphate, and 2 mM EDTA. The mixture was incubated on ice for 1 h, after which time 150 μL of 0.05 M phosphate, 1 mM EDTA, and 75 μg of bovine pancreatic trypsin inhibitor/mL were added. The mixture was immediately layered onto a 5–20% sucrose gradient (5 mL) and centrifuged at 4 °C for 4 h at 50000 rpm in a Beckman SW50 rotor. Fractions of about 0.25 mL were collected from the gradients and assayed for protein by a dye-binding assay (Bradford, 1976). The fractions corresponding to t-E2 or E2 (control) were pooled and dialyzed vs. 0.05 M phosphate containing 0.01% sodium azide.

Polyacrylamide gel electrophoresis in the presence of Na-DodSO_4 was performed in slabs containing a 12% separating gel according to the method of Laemmli (1970).

Electron Microscopy. Specimens were applied to carbon-coated grids (400 mesh) that had been glow-discharged no more than about 4 h before use. Typically 5 μL of E2 or t-E2 in 0.05 M phosphate at 50–100 μg/mL was applied to the grid. After 1 min, the grid was blotted, and 5 μL of H_2O was applied and immediately blotted. The grid was then rinsed with 5–7 drops of 1% uranyl acetate, blotted, and allowed to dry.

Electron microscopy was done with a Philips EM 301 transmission electron microscope operated at 80 kV. All micrographs were taken at a magnification of 43000×. Precautions were taken to minimize the electron dose by using a shutter attached to the first condenser aperture (Unwin & Henderson, 1975). Grids were screened, and those in which the specimen and stain were spread uniformly over large areas of the grid (at least several grid squares) were selected, because the procedure for recording minimal-dose micrographs can then be greatly simplified. With a narrow illuminating beam, the grid is scanned for a suitable area, and focusing, astigmatism, and beam intensity adjustments are made. The beam is then occluded by the shutter, the grid is translated just far enough to reach an unexposed region, the shutter is opened, and an exposure is made. With practice, minimal-dose micrographs can be obtained with little effort beyond that required for conventional-dose micrographs. The electron doses were estimated to be about 2000 e^-/nm^2, assuming the electron speed quoted by the manufacturer for Kodak 4463 electron microscope film.

Prospective micrographs were examined by optical diffraction. Those for which the astigmatism had been adequately corrected and the degree of underfocus was suitable for revealing structural detail below 2 nm were selected for further analysis by computerized image processing.

Image Processing. The micrographs were digitized on a Perkin-Elmer Model PDS1010A flatbed automatic microdensitometer. The raster size was 25 μm, which corresponds to 0.68 nm at the specimen.

All of the image-processing procedures, except correspondence analysis, were run under the SPIDER image-processing software system (Frank et al., 1981a). The methods required for averaging images of individual molecules have been described in detail elsewhere (Frank et al., 1978; 1982; Frank, 1982; Kessel et al., 1980). Only a brief description will be given here.

The first step in the analysis is to select the particles to be analyzed from the digitized micrographs. To avoid any bias in the selection of particles, an automated procedure was devised for selecting images from fields containing many molecules (Frank & Wagenknecht, 1984). The automated procedure also eliminated the laborious task of measuring the coordinates of hundreds of particles by hand or of having to select the particles by moving a cursor on a video display. The automated procedure locates the center of each enzyme molecule and isolates it from the rest of the micrograph by retaining for further analysis a square area of any desired size surrounding the molecule. The selected particles were then translationally and rotationally aligned with respect to a reference image by correlation methods (Frank et al., 1978; Frank, 1982). We routinely took advantage of the 4-fold symmetry of the E2 and t-E2 images by rotationally averaging the images. The degree to which 4-fold symmetry was obeyed for each of the images was determined by computing their rotational power spectra (Crowther & Amos, 1971).

Artifacts and loss of resolution can occur in the averaging of individual particles if factors other than noise are responsible for the differences between the images. It is therefore desirable to impose objective criteria to the set of aligned images in order to exclude from the analysis images showing large variations from the norm. Accordingly, only particles satisfying the following criteria were included in the averaging: (1) Particles should be well separated from nearby particles. (2) Particles should be in the 4-fold (face-on) view, as judged by the power contributed by 4-fold cylindrical harmonics to the rotational power spectrum. (3) Particles satisfying criteria 1 and 2, when submitted to correspondence analysis, should not be outliers in the space defined by the two or three largest eigenvectors. Correspondence analysis is a multivariate statistical method which can be used to objectively and quantitatively classify images (Frank et al., 1982; van Heel & Frank, 1981).

The resolution of an averaged image was estimated by computing the interimage phase residual between two averages computed from independent sets of images (Amos & Klug, 1975; Frank et al., 1981b). The averages for both E2 and t-E2 were reproducible to about 2.5 nm.

Before comparing averaged images obtained from different micrographs, it is necessary to compensate for differences in

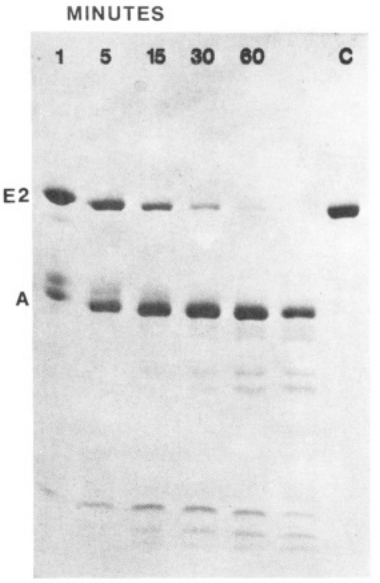

FIGURE 1: Time course of tryptic digestion of the E2 complex as monitored by polyacrylamide gel electrophoresis in the presence of $NaDodSO_4$. Purified E2 complex was modified with trypsin (see Materials and Methods), and 10-μL aliquots were withdrawn at the times indicated and added to 5 μL of trypsin inhibitor (75 μg/mL). The trypsin-modified complexes to be studied by electron microscopy were digested for 60 min.

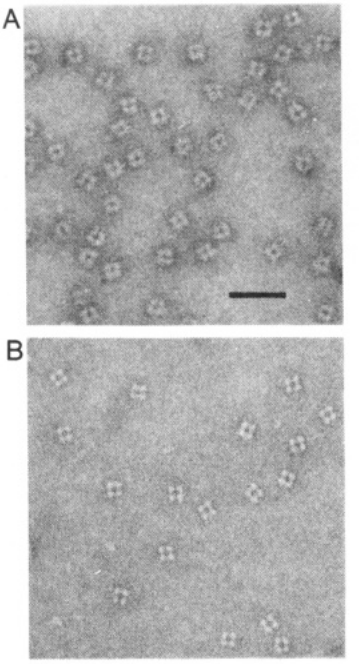

FIGURE 2: Electron micrographs of negatively stained (A) E2 and (B) t-E2. The bar represents 4.5 nm.

optical density due to trivial factors such as different exposure times. Two micrographs were scaled to one another by multiplying the optical density of each picture element of one of the micrographs by a scaling factor equal to the ratio of the average overall optical densities from the two micrographs.

Results

Removal of Lipoyl-Containing Domains from E2. Incubation of the isolated E2 with low concentrations of trypsin cleaved the constituent polypeptide chains into a stable component of M_r ~37 000 and a smaller component which undergoes further proteolysis. This behavior could be demonstrated by monitoring the proteolysis as a function of time by polyacrylamide gel electrophoresis in the presence of $NaDodSO_4$. We found, in agreement with others (Stepp et al., 1981; Perham & Roberts, 1981), that the larger protease-resistant fragment (Figure 1, band A) exists as part of a multisubunit complex which is free of the lower molecular weight components generated by the treatment with trypsin. The lipoic acid moieties are released with the lower molecular weight peptides.

Electron Microscopy of E2 and t-E2. Electron micrographs of negatively stained E2 molecules before and after incubation with trypsin are shown in Figure 2. Both types of molecules appear generally square overall and have a stain-filled hole about 4 nm in diameter at the center. Clearly the trypsin treatment does not affect the tendency of the E2 complex to lie in a preferred orientation on the carbon-supporting surface. A low-resolution three-dimensional map has been determined for the E2 complex (DeRosier et al., 1971; DeRosier & Oliver, 1971) which shows the molecule as a cube with truncated corners. The 24 polypeptide chains comprising the structure are arranged so that most of their mass is located at the 24 vertices of the truncated cube. The 4-fold rotational symmetry characteristic of most of the complexes observed in the electron micrographs has therefore been interpreted to mean that the molecules adhere preferentially to the grid by one of their faces.

Differences between the images of the native and the trypsin-modified E2 are also readily apparent. The region of strong strain exclusion (white in the micrographs) surrounding the central hole appears to be slightly thicker and more featureless for E2 than for t-E2. In t-E2, this region often appears to be divided into four distinct regions by a cross-shaped region of weaker stain exclusion. In the more extreme cases, the images appear to consist of four distinct morphologic units centered on the vertices of a square. These differences were reproducibly observed in essentially all of the micrographs recorded from several independent experiments and are not the result of variability in focus or other electron-optical parameters. To define the differences between the two types of images more precisely, it was necessary to apply computerized image-analysis methods.

Analysis of Rotational Symmetry. Molecules with rotational symmetry are most conveniently analyzed by Fourier analysis in polar coordinates in terms of cylindrical harmonics (Crowther & Amos, 1971). Fourier analysis allows an objective assessment of the degree to which rotational symmetry is obeyed for a population of molecular images. This may be expressed as the total power contributed by n-fold harmonics to the power spectrum. We found that, as we suspected from qualitative visual analysis of the images (see above), the t-E2 images have an average greater 4-fold power (ca. 65%) than the E2 images (ca. 50%).

Several explanations for this difference are possible. If the peptide removed by proteolysis does indeed function as a flexible arm for the lipoyl moiety as suggested by other work (Stepp et al., 1981; Perham & Roberts, 1981), random deviations from 4-fold symmetry are possible and could significantly reduce the power contributed by 4-fold harmonics. Alternatively, even in the absence of such deviations from 4-fold symmetry, there is no reason to expect E2 and t-E2 to exhibit the same degree of 4-fold symmetry. In E2, the mass may simply be distributed in such a way that more of the power is contained in higher order harmonics, which are beyond the resolution attained in the micrographs.

Galleries of images of E2 and of t-E2 after 4-fold rotational averaging are shown in Figure 3. The two types of molecules look much more similar to each other than they did before rotational averaging (cf. Figure 2). The main difference is

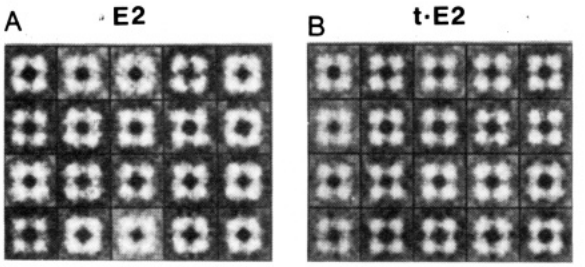

FIGURE 3: Fourfold rotationally averaged images of (A) E2 and (B) t-E2. The width of each frame represents 23 nm.

that the regions of low density between the morphological units forming the corners of the molecules are better defined in the t-E2 than in the E2 images. This effect can be seen by defocusing one's eyes and viewing several images of the modified E2 or native E2 simultaneously. The central hole and low-density regions between the corner morphological units form a dark plus sign (+), which is generally more pronounced in the t-E2 images. The close similarity of E2 and t-E2 after rotational averaging implies that at least part of the difference observed between the nonaveraged images is due to structural differences that do not obey 4-fold symmetry. This is, of course, consistent with the idea that the lipoyl-bearing domains which are present in E2 and absent from t-E2 are not rigidly bound to the complex.

Computed Averages of E2 and t-E2 in Face-On Orientation. Computed averages of the E2 and t-E2 complexes are shown in Figure 4a,b. In gross appearance the two averages are, as expected, very similar, each having four large, circular, strongly stain-excluding lobes centered at vertices defining a square. In both averages, the central region appears filled with stain and is about 5 nm in diameter. The major difference is seen along the edges in the regions connecting the four strongly stain-excluding regions: more mass appears in these areas for E2 than for t-E2.

These differences are more easily discernible in the difference image (Figure 4c), where the density scaling has been expanded about 5-fold to accentuate the differences. Here the differences along the edges are distinct, localized regions. The size of these regions is difficult to determine because there is no sharp defining boundary, but we estimate a diameter of 3–5 nm.

These regions are slightly skewed in shape, and consequently, the difference map lacks the *mm* symmetry expected of the octahedrally symmetric E2 molecule when viewed in projection along one of the 4-fold symmetry axes. This behavior probably arises because of a slight nonequivalence between the sides of the E2 molecules in contact with the carbon support surface relative to the opposite sides; such nonequivalences are commonly induced during negative staining [for further examples and discussion of this point, see Frank et al. (1978)].

Aside from the four main density maxima, the difference map is rather featureless. There is evidence of weaker density differences in regions corresponding to the center and at the corners of the E2 molecule as viewed in the 4-fold projection, but these differences are not regarded as significant.

As a check on the reliability of the averages, we show for comparison the model for E2 derived from X-ray crystallography (DeRosier & Oliver, 1971; DeRosier et al., 1971). Figure 4d shows the X-ray model as viewed in projection along one of its 4-fold symmetry axes and displayed at the same resolution (2.5 nm) as the averages of the negatively stained E2 and t-E2.[2] The X-ray model is perhaps more directly

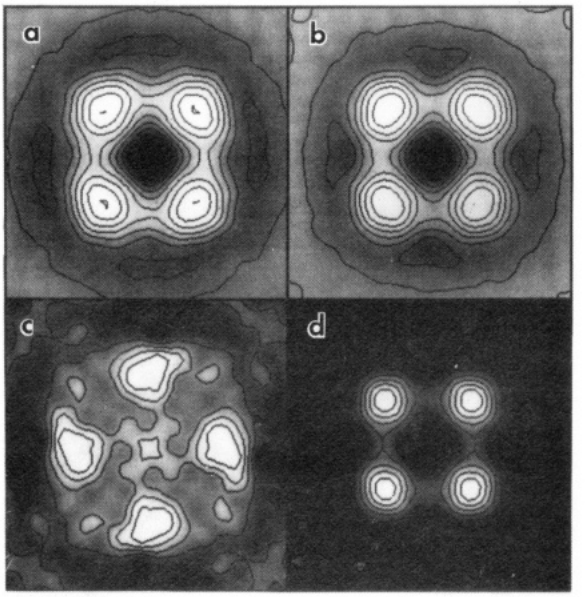

FIGURE 4: Computer averaging of E2 and t-E2 images. (a) Average of 62 E2 images. (b) Average of 60 t-E2 images. In (a) and (b), the maximum optical density is 0.73, and the contours are spaced at intervals of 0.015 ODU. (c) Difference image obtained by subtracting (b) from (a). The maximum optical density in (c) is 0.018, and the contours are spaced at intervals of 0.005 ODU. (d) Projection of E2 molecule in the 4-fold orientation as derived from the three-dimensional model of DeRosier et al. (DeRosier & Oliver, 1971; DeRosier et al., 1971). The width of each frame corresponds to 23 nm.

comparable with the average image of the t-E2 complex (Figure 4b), because during crystallization proteolysis probably occurred, presumably at or near the site of tryptic cleavage (D. J. DeRosier and L. J. Reed, personal communications). The only significant difference between the X-ray model and the models obtained by single-particle averaging is the smaller size (by about 6%) of the former. This discrepancy is probably due to a slight flattening of the negatively stained E2 complexes. Otherwise the close similarity of the averaged images to the X-ray model shows that single-particle averaging methods applied to negatively stained specimens can give a faithful representation of molecular structure in the 2–3-nm resolution range.

Analysis of Micrographs Containing both E2 and t-E2 Complexes. Could the differences observed between E2 and t-E2 be trivial artifacts due to the fact that images from different micrographs were compared? For example, the properties of negative stains such as uranyl acetate depend on factors (e.g., the hydrophobicity of the grid) that are difficult to control, and frequently the staining is not uniform, even between regions on the same grid. Thus, differences between images obtained from different grids could be due to differences in staining, rather than genuine structural variation. It is also necessary to scale the micrographs being compared, with respect to both magnification and average density, and errors in scaling can affect the differences observed. We ruled out these possibilites by showing that when E2 and t-E2 were mixed together and applied to a grid, the same differences were observed as when the two were analyzed independently.

Ideally we would like to be able to separate images of E2 and t-E2 in the same field, compute their averages, and find the differences between them, just as was done above when the two types of images were obtained from separate micro-

[2] The projection derived from X-ray crystallography is not strictly comparable to that obtained by electron microscopy using negative stain because the source of contrast in the two methods is very different. However, at low resolution, a direct comparison is probably valid.

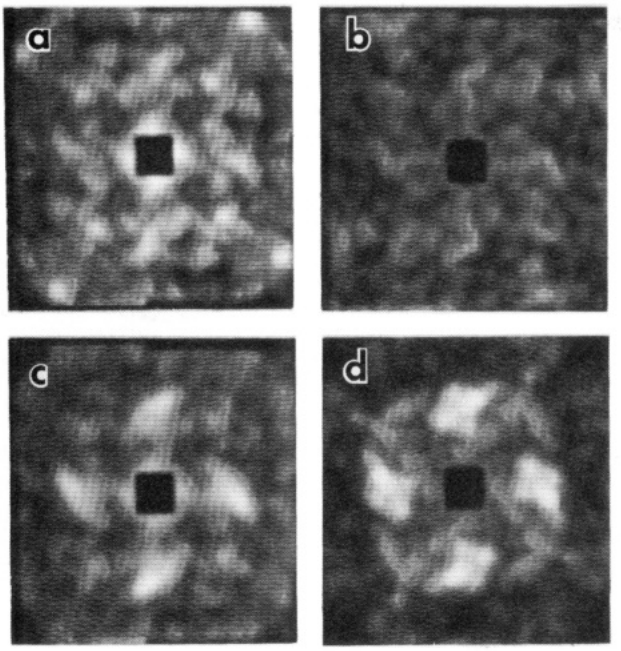

FIGURE 5: Variance maps for populations of (a) E2 images ($N = 98$) and (b) t-E2 images ($N = 98$). (c) Variance map for the combined populations of (a) and (b). (d) Variance map for a mixture of E2 and t-E2 molecules present in a single micrograph ($N = 126$). All images were 4-fold rotationally averaged prior to computation of the variances. The maxima in (c) and (d) correspond to standard deviations of 0.016 optical density unit. The width of each map corresponds to 23 nm.

graphs. Unfortunately, when the two types of complex are present on the same grid, it is difficult to classify them visually because the degree of variability within each of the classes is comparable to the differences between classes. However, we can form the average of the total population of images and determine the relative variance for each density point on the average. If the population consists of two classes of images and these differ from each other in a systematic way, the regions of the images characterizing the difference will show up as regions of high variance in the average, provided the differences are larger than the variations experienced within either class.

The variance maps for averages of E2 and t-E2 as obtained from separate micrographs are shown in Figure 5a,b. The variance map obtained when the images which contributed to the two independent averages were pooled together and averaged is shown in Figure 5c. This variance map for the combined images is dominated by regions of high variance at the same locations as the main peaks in the difference map between t-E2 and E2 (Figure 4c), while the variance maps for E2 and t-E2 show weaker modulations in these regions relative to the other areas in the image. Thus, when images of E2 and t-E2 obtained from separate micrographs were combined and averaged, the variance map shows regions of high variation in precisely those areas where E2 and t-E2 differ most.

The variance map obtained from a micrograph of an equimolar mixture of E2 and t-E2 complexes is shown in Figure 5d. The regions of high variation agree with those obtained when E2 and t-E2 were artificially combined (Figure 5c). We conclude that the differences between the t-E2 and E2 averages (Figure 4a,b) are not an artifact arising because different micrographs were used. An alternative strategy for distinguishing images of E2 from t-E2 is to apply correspondence analysis [Materials and Methods; see also Frank et al. (1982) and van Heel & Frank (1981)] to the images after 4-fold rotational averaging. The results of such an analysis (data not shown) also demonstrated that the major source of variation between the two image types arose from regions of the molecule corresponding to the main peaks found in the difference map of Figure 4c.

Discussion

In this paper, we have compared the structures of the E2 complex isolated from the KGDC of *Escherichia coli* before and after treatment with trypsin under controlled conditions. We find, in agreement with others (Stepp et al., 1981; Perham & Roberts, 1981), that trypsin removes quantitatively a peptide of $M_r \sim 11\,000$ from the complex without disrupting its basic architecture. Single-particle averaging methods were applied to images of the E2 and t-E2 molecules, both of which preferentially adhere to the carbon-supporting surface in an orientation showing 4-fold rotational symmetry. Four regions of excess stain exclusion were found for E2 relative to t-E2. These regions appeared as roughly circular lobes about 4 nm in diameter, situated at the centers of the edges of the E2 molecule as viewed in the 4-fold orientation. We interpret these regions as representing the mass lost by the E2 molecule after treatment with trypsin. We will refer to the peptide removed by trypsin as the lipoyl peptide or lipoyl domain, since the lipoic acid moieties are contained in the peptide released by trypsin.

Possibility of Artifacts. As with all studies of protein structure by the negative-staining technique, there is a possibility of artifacts. Fortunately, E2 has been characterized by other physical and chemical techniques, so the reliability of at least some of our interpretations can be checked. Of special importance is the three-dimensional electron density map of the E2 complex derived from X-ray crystallography (DeRosier & Oliver, 1971; DeRosier et al., 1971; Hainfeld, 1974). The average image of t-E2 determined by image averaging is remarkably similar to that found for the unstained molecule by X-ray diffraction (cf. Figure 4b,d). Since our aim is to map the positions of the lipoyl domains on the surface of the E2 molecule rather than to determine their detailed structure, no significant error is likely to result, even if the lipoyl peptides are denatured in the negative stain.

Another potential pitfall in comparing similar structures from different micrographs is the variability in the negative staining between grids. We have ruled out this artifact as responsible for the differences between E2 and t-E2 by showing that the same differences were observed when E2 and t-E2 were present together on a grid.

Three-Dimensional Mapping of Lipoyl Domains on the E2 Molecule. Although we have compared the E2 and t-E2 complexes in only one orientation, it should be possible, because of the high symmetry of the molecule, to determine the locations of the lipoyl domains in three dimensions. However, as we discuss below, this analysis is hampered because not all of the lipoyl peptides are represented in the difference map.

The main regions of excess density in E2 relative to t-E2 are four equivalent regions centered along the edges of the molecule, as viewed in projection and in the 4-fold orientation (Figure 4). In three dimensions, these positions are consistent with the lipoyl domains being located anywhere along a line connecting the midpoints of oppositely related edges on the faces of a cube-shaped E2 molecule. The three-dimensional model for E2 derived by crystallography shows no mass on the faces and is therefore consistent with the lipoyl domains being located along the edges. However, as discussed earlier, it is likely that during crystallization E2 was modified by endogenous proteases and so the modified E2 may actually more closely resemble t-E2 than E2. Nevertheless, we still

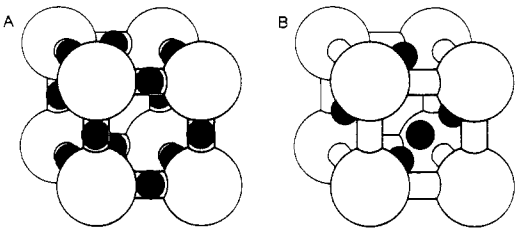

FIGURE 6: Two schematic models for arrangement of lipoyl domains in the E2 complex. In model A, each black sphere represents two lipoyl domains and should be interpreted as embedded in the pegs connecting the large white spheres. In model B, the black spheres each represent four lipoyl domains and are located on faces of the E2 molecule. An E2 polypeptide chain, not including the lipoyl domain, is represented by one-third of a large sphere and half of a connecting peg.

favor a model in which the lipoyl domains are located along the edges, for the reasons discussed below.

Let us consider the following two extreme cases: the lipoyl domains are located near the midpoints of the edges of the E2 molecule (Figure 6, model A), and the domains are situated near the centers of the faces of the E2 molecule (model B). Both of these possibilities imply that additional regions of density should have been observed in the difference image (Figure 4c) besides the four equivalent regions discussed. Viewing the molecules face-on and in projection, we should have observed densities corresponding to the corners of E2 for model A and additional density at the center for model B. Since we did not observe significant differences in density at these regions, some of the lipoyl domains are not being resolved in the difference image. In order to determine where the lipoyl domains are located in three dimensions, we must therefore consider additional structural information and make some reaonable assumptions.

Despite this lack of some expected densities, the difference image between E2 and t-E2 is more consistent with model A than with model B. Since there are 24 lipoyl domains per molecule, each of the 12 lipoyl-containing regions of model A must represent two lipoyl peptides, while for model B each of the six regions must represent four lipoyl peptides. When viewed face-on and in projection, both models are consistent with regions of density corresponding to four lipoyl domains along the edges, exactly as in the difference image. For model A, this pattern occurs because the lipoyl-containing regions from the top and bottom of the molecule are superposed. There should be additional regions of the density at the corners, but since these regions correspond to just two lipoyl peptides each, it is reasonable that they might not be detected in our analysis.

For model B, additional regions of density, representing eight lipoyl peptides, should be observed in the central regions of the difference image, and it is unlikely that this density could have gone undectected. Furthermore, the centrally located mass predicted for model B falls in a region of the image of the E2 molecule characterized by an overall low level of mass density, where its detection should be favorable, while the mass expected at the corners for model A falls in regions of very high density, making detection more difficult.

If the lipoyl domains function as flexible arms capable of allowing large translational movements of the lipoyl moieties (Stepp et al., 1981; Perham & Roberts, 1981), then the interpretation of the differences we have detected between E2 and t-E2 is somewhat complicated. When averages from images of single particles are formed, regions of the molecule exhibiting large random translational movements will behave much like noise and may not be detected. The fact that significant density differences were detected could mean that only a relatively nonmobile part of the domain cleaved by trypsin is being visualized or, alternatively, the differences could represent a kind of probability distribution over many orientations and relative arrangements of the lipoyl domains. If the former interpretation is correct, then it is likely that the regions of the flexible arms near the points of attachment to the main body of the E2 molecule are being detected, since translational mobility would be restricted by the shortness of the tether in this region. A similar situation was found in a recent study in which antigenic sites on hemocyanin complexes were mapped by comparing averages of complexes either having or lacking a bound antibody; only a part of the bound antibody, corresponding to the antigen binding region, was visible in difference maps (Frank et al., 1983). If the difference image between E2 and t-E2 is indeed highlighting the regions where the lipoyl peptides are joined to E2, then the only possible locations in three dimensions for these regions are along the edges. This follows because the three-dimensional model for (protease-modified) E2 (DeRosier & Oliver, 1971; DeRosier et al., 1971) shows no mass in the regions between the edges (i.e., on the faces).

In an earlier study, we found that the E1 and E3 subunits also bind to the E2 complex near the midpoints of its edges (Wagenknecht et al., 1983). This close proximity of the lipoyl domains to E1 and E3 is consistent with one of their presumed functions, to transfer the various reaction intermediates among the active sites of the three components. Our proposed model for the arrangement of the lipoyl domains on E2 is also consistent with the results of a recent study in which the activity of the KGDC was monitored as a function of the number of functional lipoyl domains (Stepp et al., 1981). The data were interpreted in terms of a model in which each E1 chain is serviced by two lipoyl domains (Hackert et al., 1983). In our structural model, the lipoyl domains occur in pairs along the edges of E2, very near the sites where the E1 subunits bind. We suggest that each pair of lipoyl peptides is capable of servicing an E1 subunit.

Our results also have implications for the nature of the extensive network of interacting lipoyl moieties. The model we are proposing places the lipoyl domains related by 2-fold symmetry (i.e., the pairs of lipoyls along the edges) in close proximity to one another (within ca. 2 nm), while the distances between the domains related by the 3-fold and 4-fold symmetry axes are rather large (5–8 nm). Clearly, interactions between lipoyls related by 2-fold symmetry are possible; the lipolyls are attached to the ϵ-amino group of lysine residues and are thought to function as swinging arms, having a maximal extension of 1.4 nm. The modeling studies (Hackert et al., 1983) require interactions between lipoyls related by 3-fold and/or 4-fold symmetry. If our structural model is correct, one function of the lipoyl peptides must be to increase the reach of the lipoyl moieties, thereby allowing interactions between lipoyl domains related by 3-fold or 4-fold symmetry.

Acknowledgments

We thank N. Francis (Brandeis University) for preparing the E2 used in this study, D. J. DeRosier (Brandeis University) for supplying an electron density map of E2 in the face-on projection, and A. Verschoor for help with the image processing.

Registry No. E2, 9032-28-4; KGDC, 9031-02-1; lipoic acid, 62-46-4.

References

Amos, L. A., & Klug, A. (1975) *J. Mol. Biol. 99*, 51–73.
Angelides, K. J., & Hammes, G. C. (1979) *Biochemistry 18*,

5531–5537.
Bates, D. L., Danson, M. J., Hale, G., Hooper, E. A., & Perham, R. N. (1977) *Nature (London) 268*, 313–316.
Bleile, D. M., Munk, P., Oliver, R. M., & Reed, L. J. (1979) *Proc. Natl. Acad. Sci. U.S.A. 76*, 4385–4389.
Bradford, M. M. (1976) *Anal. Biochem. 72*, 248–254.
Collins, J. H., & Reed, L. J. (1977) *Proc. Natl. Acad. Sci. U.S.A. 74*, 4223–4227.
Crowther, R. A., & Amos, L. A. (1971) *J. Mol. Biol. 60*, 123–130.
Danson, M. J., Fersht, A. R., & Perham, R. N. (1978) *Proc. Natl. Acad. Sci. U.S.A. 75*, 5386–5390.
DeRosier, D. J., & Oliver, R. M. (1971) *Cold Spring Harbor Symp. Quant. Biol. 36*, 199–203.
DeRosier, D. J., Oliver, R. M., & Reed, L. J. (1971) *Proc. Natl. Acad. Sci. U.S.A. 68*, 1135–1137.
Frank, J. (1982) *Optik (Stuttgart) 63*, 67–89.
Frank, J., & Wagenknecht, T. (1984) *Ultramicrosopy 12*, 169–176.
Frank, J., Goldfarb, W., Eisenberg, D., & Baker, T. S. (1978) *Ultramicroscopy 3*, 283–290.
Frank, J., Shimkin, B., & Dowse, H. (1981a) *Ultramicroscopy 6*, 343–358.
Frank, J., Verschoor, A., & Boublik, M. (1981b) *Science (Washington, D.C.) 214*, 1353–1355.
Frank, J., Verschoor, A., & Boublik, M. (1982) *J. Mol. Biol. 161*, 107–137.
Frank, J., Sizaret, P. Y., Verschoor, A., & Lamy, J. (1983) *Proc.—Annu. Meet., Electron Microsc. Soc. Am. 41*, 282–283.
Hackert, M. L., Oliver, R. M., & Reed, L. J. (1983) *Proc. Natl. Acad. Sci. U.S.A. 80*, 2226–2230.
Hainfeld, J. F. (1974) Ph.D. Thesis, The University of Texas, Austin, TX.
Kessel, M., Frank, J., & Goldfarb, W. (1980) *J. Supramol. Struct. 14*, 405–422.
Koike, M., Reed, L. J., & Carroll, W. R. (1963) *J. Biol. Chem. 238*, 30–39.
Laemmli, U. K. (1970) *Nature (London) 227*, 680–685.
Oliver, R. M., & Reed, L. J. (1982) in *Electron Microscopy of Proteins* (Harris, J. R., Ed.) Vol. 2, pp 1–48, Academic Press, London.
Perham, R. N., & Roberts, G. C. K. (1981) *Biochem. J. 199*, 733–740.
Perham, R. N., Duckworth, H. W., & Roberts, G. C. K. (1981) *Nature (London) 292*, 474–477.
Pettit, F. H., Hamilton, L., Munk, P., Namihira, G., Eley, M. H., Willms, C. R., & Reed, L. J. (1973) *J. Biol. Chem. 248*, 5282–5290.
Reed, L. J., & Oliver, R. M. (1968) *Brookhaven Symp. Biol. No. 21*, 397–411.
Reed, L. J., & Mukherjee, B. B. (1969) *Methods Enzymol. 13*, 55–61.
Stepp, L. R., Bleile, D. M., McRorie, D. K., Pettit, F. H., & Reed, L. J. (1981) *Biochemistry 20*, 4555–4560.
Unwin, P. N. T., & Henderson, R. (1975) *J. Mol. Biol. 94*, 425–440.
van Heel, M., & Frank, J. (1981) *Ultramicroscopy 6*, 187–194.
Wagenknecht, T., & Frank, J. (1983) *Proc.—Annu. Meet., Electron Microsc. Soc. Am. 41*, 756–757.
Wagenknecht, T., Francis, N., & DeRosier, D. J. (1983) *J. Mol. Biol. 165*, 523–541.
Waskiewicz, D. E., & Hammes, G. G. (1982) *Biochemistry 21*, 6489–6496.

Tests of the Simple Model of Lin and Brandts for the Folding Kinetics of Ribonuclease A†

Franz X. Schmid, Michael H. Buonocore, and Robert L. Baldwin*

ABSTRACT: L.-N. Lin and J. F. Brandts recently proposed a simple model for the folding kinetics of ribonuclease A in which folding intermediates are not detectable. We have tested the basic assumption of the simple model for the major unfolded species, which is produced by a slow isomerization (the "X ⇌ Y reaction" according to Lin and Brandts) after unfolding. The simple model assumes that in refolding the slow Y → X reaction must occur before any folding can take place. We have measured the Y → X reaction during folding. Tyrosine-detected folding occurs before the Y → X reaction; the difference in rate between the Y → X reaction and folding monitored by tyrosine absorbance becomes large when the stabilizing salt 0.56 M $(NH_4)_2SO_4$ is added. The simple model predicts that the kinetic properties of the X ⇌ Y reaction in unfolded ribonuclease are the same as those of tyrosine-detected folding. We find, however, that the kinetics of the X ⇌ Y reaction in unfolded ribonuclease are independent of urea concentration, whereas the rate of tyrosine-detected folding decreases almost 100-fold between 0.3 and 5 M urea, as reported by Lin and Brandts. We point out that the kinetic properties of the X ⇌ Y reaction in unfolded ribonuclease are characteristic of proline isomerization.

Recently, L.-N. Lin and J. F. Brandts developed a new method, isomer-specific proteolysis, for studying the cis ⇌ trans isomerization of proline residues after a protein unfolds. It can be used to test the hypothesis (Brandts et al., 1975) that proline isomerization accounts for the existence of both fast-folding (U_F)[1] and slow-folding (U_S) forms of an unfolded protein, a phenomenon first observed for RNase A (Garel &

† From the Institute of Biophysics and Biophysical Chemistry, University of Regensburg, Regensburg, West Germany (F.X.S.), and the Departments of Electrical Engineering (M.H.B.) and Biochemistry, Medical Center (R.L.B.), Stanford University, Stanford, California 94305. *Received November 22, 1983.* This research was supported by grants from the Deutsche Forschungsgemeinschaft (Schm 444/2-1 to F.X.S.) and from the National Institutes of Health (GM 19988-22 to R.L.B.).

[1] Abbreviations: RNase A, bovine pancreatic ribonuclease A (EC 3.1.27.5) with disulfide bonds intact; U_S and U_F, slow- and fast-folding species of unfolded RNase A; N, native RNase A; f_{CX}, fraction of RNase A molecules with native (C and X) isomers; Gdm, guanidinium.

0006-2960/84/0423-3389$01.50/0